JASA ARTICLE

Experimental analysis of the acoustic field of an ultrasonic pulse induced by a fluidic switch

Benjamin Bühling,[1,a] Christoph Strangfeld,[1] Stefan Maack,[1] and Thorge Schweitzer[2]
[1]*Bundesanstalt für Materialforschung und -prüfung (BAM), Unter den Eichen 87, 12205 Berlin, Germany*
[2]*FDX Fluid Dynamix GmbH, Rohrdamm 88, 13629 Berlin, Germany*

ABSTRACT:
Ultrasonic inspection is a common tool for non-destructive testing in civil engineering (NDT-CE). Currently, transducers are coupled directly to the specimen surface, which makes the inspection time-consuming. Air-coupled ultrasound (ACU) transducers are more time-efficient but need a high pressure amplitude as the impedance mismatch between the air and the concrete is high and large penetration depth is needed for the inspection. Current approaches aim at eliminating the impedance mismatch between the transducer and the air to gain amplitude; however, they hardly fulfill the NDT-CE requirements. In this study, an alternative approach for ultrasound generation is presented: the signal is generated by a fluidic switch that rapidly injects a mass flow into the ambience. The acoustic field, the flow field, and their interaction are investigated. It is shown that the signal has dominant frequencies in the range of 35–60 kHz, and the amplitude is comparable to that of a commercial ACU transducer.
 https://doi.org/10.1121/10.0003937
(Received 11 November 2020; revised 5 March 2021; accepted 8 March 2021; published online 1 April 2021)
[Editor: Michael R. Haberman] Pages: 2150–2158

I. INTRODUCTION

Today, civil infrastructure is estimated to account for 50% of industrialized countries' assets (Long *et al.*, 2008). Nevertheless, these structures suffer from aging and degeneration, including yearly repair costs of 8.3×10^9 dollars only for highway bridges in the United States and 13×10^9 euros for the whole German transport infrastructure (Koch *et al.*, 2002; Kunert and Link, 2013). Thus, infrastructure needs to be inspected regularly for proper maintenance. Methods for non-destructive testing in civil engineering (NDT-CE) include, e.g., ground penetrating radar, thermography, ultrasonic techniques, etc. (Maierhofer *et al.*, 2010).

Ultrasonic inspection using body waves is commonly and successfully used to detect damages, determine material properties, and locate reinforcements in reinforced concrete. Measurements require a high pressure amplitude to penetrate specimens in centimeter-to-meter scale. Center frequencies of less than 100 kHz are typically used to avoid scattering by aggregates added to the cement (Krautkrämer and Krautkrämer, 1990; Popovics *et al.*, 2000), although use of higher frequencies has been reported (Jacobs and Whitcomb, 1997; Popovics *et al.*, 2000). In industrial practice, an investigator examines critical locations of a structure with a handheld ultrasonic device that is pressed against a concrete surface for direct coupling (Schickert and Krause, 2010). While being commercially available and providing useful high-quality three-dimensional information of the specimen, this procedure is time consuming, and thus only selected areas are investigated. Extensive measurements of entire structures are therefore too expensive to be economically feasible.

To lift this limitation, air-coupled ultrasound (ACU) methods are being developed, which would enable fast and automatable non-contact measurements (Gräfe and Krause, 2006). The main challenge in generating ACU is the enormous amplitude loss of the signal. As a very compliant medium, air has an acoustic impedance that is about three orders of magnitude lower compared to the material of the transducer and that of the specimen. This leads to high amplitude losses at the transducer-air and air-specimen interfaces. While the losses at the latter are a result of the ACU setup itself, losses at the transducer have been the subject of research since ACU methods were first applied to non-destructive testing (NDT) in the early 1970s (Luukkala *et al.*, 1971).

In practice, piezoelectric and capacitive transducers are most commonly used to generate ACU signals (Chimenti, 2014). Both use pressure-volume work to generate sound. Piezoelectric transducers use piezoelectric crystals coated with thin layers for acoustic impedance matching, whereas capacitive transducers use electrostatically excited membranes to perform this work. Commercially available transducers suffer a transmission loss of 98.2% of the sound pressure (Gräfe, 2009). While these types of actuators are still being improved (Hansen *et al.*, 1999; Álvarez-Arenas and Díez, 2013; Qiu *et al.*, 2015), a third type of resonant transducers based on ferroelectrets has emerged recently. These transducers provide low acoustic impedance but have their optimum center frequency at 250 kHz (Bovtun *et al.*,

[a]Electronic mail: benjamin.buehling@bam.de

https://doi.org/10.1121/10.0003937

2007; Gaal *et al.*, 2019), which is too high for most measurement tasks in civil engineering.

In the past ten years, novel techniques have emerged aiming at ACU generation without any vibrating surfaces by utilizing the thermoacoustic effect. Daschewski *et al.* (2013) pursued a concept proposed by Shinoda *et al.* (1999) to generate ultrasonic pulses by Ohmic heating of an electrically conductive film results in a single broadband ultrasonic pulse ranging from 1.2 kHz to 1 MHz (Bente *et al.*, 2018). By applying an electrode voltage of 1.5 kV, a sound pressure level of 115 dB is reached at a frequency of 50 kHz (Daschewski *et al.*, 2013). Kotschate *et al.* (2018a,b) proposed to combine pressure-volume work with the thermoacoustic effect for sound generation by utilizing plasma discharges. Generating pulses with dominant frequencies below 100 kHz, this type of transducer reaches up to 137 dB SPL when operated at a peak-to-peak voltage of 4 kV. Dai *et al.* (2013) used a spark source to generate a broadband low frequency ultrasonic pulse for impact-echo measurements, reaching 450 Pa when unmodified and more than 3000 Pa when focused using an elliptic reflector.

Further research has used short pulsed lasers to generate broadband acoustic waves by various mechanisms directly at the specimen surface, which avoids transmission loss (Hutchins, 1988) and has also been shown to work for transmission measurements in concrete (Jacobs and Whitcomb, 1997). A drawback of the method is material ablation that may occur due to the high power laser needed (Davies *et al.*, 1993). A high power microwave source has also been used to achieve ultrasonic excitation by local heating (Hosten and Bernard, 1998; Hosten *et al.*, 2002). X-ray induced ultrasound offers another mechanism for non-contact ultrasound generation (Kim and Sachse, 1983; Tang *et al.*, 2018; Robertson *et al.*, 2020). Here, the ultrasonic waves are generated by heating at the defect location itself and therefore have a shorter travel time in the specimen, decreasing their damping. The method promises high resolution imaging; however, high levels of X-ray energy are needed in low ultrasonic regimes, which may damage the equipment.

In addition to increasing the signal strength for increased performance of ultrasonic testing, progress has been made in terms of pulse compression (Purnell *et al.*, 2004; Berriman *et al.*, 2006; Hutchins *et al.*, 2014; Laureti *et al.*, 2018) and reconstruction techniques (Mayer *et al.*, 1990; Schickert *et al.*, 2003; Asadollahi and Khazanovich, 2018), which allow for a strong increase in signal-to-noise ratio without increasing the emitted pressure amplitude.

The research presented here aims at providing insight into the sound field of the novel fluidic ultrasonic transducers. Similar to thermoacoustic and plasma transducers, fluidic transducers aim at generating ACU without an impedance mismatch between transducer and the surrounding air. However, the working principle is based solely on volume work and does not require any high voltage supply, laser safety precautions, and does not cause material ablation or potentially harmful radiation, which may restrict the use outside a lab environment.

The knowledge about the acoustic characteristics presented in this study lays the ground work for the development of a full NDT system for concrete specimens and further development of fluidic transducers for other fields of application. In Sec. II, fluidics technology is outlined with a focus on the fluidic switch, which is used in this study to generate ultrasound, and its properties, that make it particularly suitable for NDT-CE. Section III describes the measurement design that is used to characterize the fluidic transducer. In Sec. IV, the measured acoustic and flow fields and their interaction are discussed. The results are compared to a commercial ACU transducer, which has been used in NDT-CE in previous studies (Gräfe, 2009; Maack, 2012).

II. THEORY

Fluidic devices, although developed in the 1960s (Warren, 1962a,b; Spyropoulos, 1964), have offered possible solutions to many modern engineering problems. They are used in active flow control (Woszidlo and Wygnanski, 2011; Gregory and Tomac, 2013) and research has been done in the realization of the shockless explosion combustion (Bobusch, 2015) or the generation of microbubbles in bioreactors (Tesař, 2002). Extensive information, history of fluidic devices, and further examples can be found in the works of Gregory and Tomac (2013), Tesař (2007), Kirshner and Katz (1975), or Bobusch *et al.* (2013). It has been shown that fluidic elements may produce significant characteristic acoustic pressures (Hirsch and Gharib, 2018), which, however, are considered to be a secondary effect. While using steady jet noise for ultrasound generation has been described by McBride and Hutchison (1976), the idea to generate ultrasound with a controllable frequency content was patented by Strangfeld and Maack (2018). The first approach to utilize sound generated by fluidic oscillators in NDT was presented by Bühling *et al.* (2019).

The fluidic transducer used in this study to generate an acoustic signal is a bistable fluidic switch (Warren, 1962b). It allows the rapid switching of a large mass flow of pressurized air (S) between two outlets (O1, O2) by applying significantly smaller mass flows at the control ports (C1, C2). The working principle of the device is presented in Fig. 1. If a constant supply pressure is applied only to S, the flow will attach to one of the outlet channels due to the Coandă effect. To determine the initial switching state with outflow through O1, a control pressure is applied to C1 [Fig. 1(a)]. The flow is then in a stable state that is preserved even when the control port is turned off [Fig. 1(b)]. To switch the state, the C2 needs to be activated. The main flow from S is then deflected [Fig. 1(c)] and reaches a new stable state exiting through the O2 [Fig. 1(d)]. The time that it takes the flow to switch between the stable states is the switching time t_s. It is mainly determined by the geometry of the switch, the internal flow velocity and the pressure applied to the control ports (Kirshner and Katz, 1975; Rechten, 1976). Thereby, the influence of the control pressure decreases asymptotically with the increasing pressure. The pressurized air

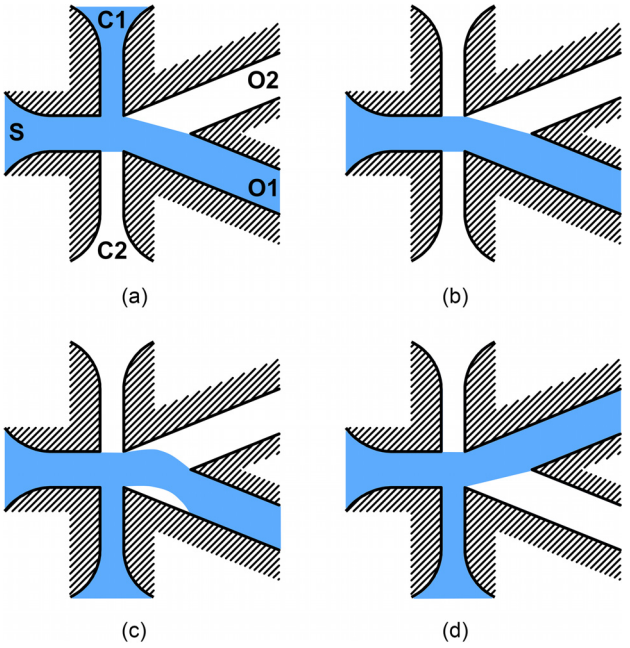

FIG. 1. (Color online) Switching process of a fluidic switch. The flow is illustrated in blue. S, pressure supply port; C1, control port 1; C2, control port 2; O1, outlet 1; O2, outlet 2. The abbreviations apply to all insets.

applied to the control ports is regulated by external valves. The switching time of these valves does not influence t_s. Once the pressure exceeds the threshold needed to detach the flow from one wall and push it to the opposite one, t_s depends only on the switching behavior of the fluidic switch. Thus, t_s is only limited by the maximum internal flow velocity that can be achieved and by the size of the device.

Since a fluidic switch allows for rapid switching of mass flow, it may be used as an ultrasonic generator. When the outlet ports start to lead the flow into ambient air, the switching initiates fast insertion of mass. This process is modelled as an acoustic point mass source. According to Pierce (2019), the acoustic pressure p at a time t of such source can be described as

$$p = \frac{1}{4\pi r}\frac{d\dot{m}\left(t-\frac{r}{c}\right)}{dt}, \tag{1}$$

where r is the radial distance from the source, c is the speed of sound, and $\dot{m}(t)$ is the inserted mass flow function. The change of mass flow $d\dot{m}/dt$ only takes nonzero values during the switching process, thus $p \propto 1/t_s$ for a fixed $\dot{m}$ and $p \propto \dot{m}$ for a fixed t_s. The generated acoustic frequency f depends on the frequency of $\dot{m}(t)$. During both switching events, pressure pulses are generated. Switching *on* produces a positive mass flow to the ambient air, switching *off* produces a negative flow. If we expand this model to a finite piston in a rigid baffle, we can observe the spherical wave radiation shifting towards a higher directivity as ka increases (Pierce, 2007), where $k = 2\pi f/c$ is the wavenumber and a is the piston radius.

The wide range of frequencies that are possible to produce and the absence of an impedance mismatch are the acoustic advantages of fluidic switches over the existing transducer technologies for ultrasound generation. Fluidic devices have further properties that make them suitable for ACU applications, especially in civil engineering: Fluidic elements are shock resistant and contain no electrical components thus they are well suited for use in harsh environments. Moreover, they are insensitive to radiation; temperature changes, however, may affect the switching properties but not the functionality of the device. As long as the supplied gas is clean, fluidic switches are also insensitive to contamination (on a construction site, for example). Additionally, they are maintenance free due to the absence of moving parts. No high voltages are needed to generate high amplitude ultrasound as the device is only powered by pressurized air.

III. MATERIALS AND METHODS

The fluidic switch studied here was designed by the company FDX Fluid Dynamix based on the bistable fluidic amplifier by Bobusch (2015) and manufactured at BAM (Fig. 2). Static pressures of 1.85 and 1.2 bar were applied continuously to the S and C2, respectively, pushing the flow to O2. The pressure applied to C1 was switched between zero-pressure and 1.4 bar. This configuration enables an automatic switch back to O1 as soon as the pressure at C1 is removed. To control the pressure at C1 a Festo MHJ10 solenoid valve is used. This device is designed to switch on within 0.8 ms; however, it has a switching time jitter of 0.24 ms. The pressure on control port 1 was switched on for a period of 15 ms with a repetition rate of 25 Hz. Only pulses emitted by switching to outlet 1 are considered here, thus this state is further referred to as *on* state. When the flow goes through outlet 2, it is referred to as the *off* state. The complete measurement setup is shown in Fig. 3. The acoustic signal was measured using a calibrated 1/4 in. (6.35 mm) MK301 microphone in combination with a MV302 preamplifier from the company Microtech Gefell, which has an almost linear impulse response up to 70 kHz and is calibrated up to 100 kHz and a sensitivity of 5 mV/Pa. The expanded uncertainty of the microphone in amplitude and

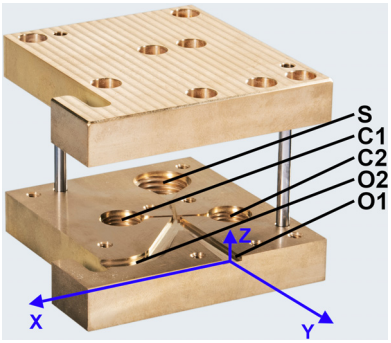

FIG. 2. (Color online) Fluidic transducer with coordinate system (blue). Abbreviations as in Fig. 1.

https://doi.org/10.1121/10.0003937

frequency is 0.15 dB and 0.1 Hz, respectively. As a reference ultrasound generator, the piezoelectric transducer NCG100-S63 from the company Ultran Group with active surface dimensions of 63×63 mm was investigated, which was driven by an 80 kHz pulse of 100 Vpp. This transducer uses as a gas matrix piezoelectric composite and is specifically designed for ACU applications (Kunkle *et al.*, 2006). Flow measurements were conducted using a one-dimensional hot-wire from the company Dantec with an IFA-100 constant temperature anemometer. The hot-wire was aligned with the z-axis so that the absolute pressure in the x- and y-direction was measured. Additionally, a Pitot tube connected to a HDOB005 pressure sensor from the company First Sensor with a range of 0–5 bar was used for flow measurement. The Pitot tube was directed in the negative y-direction so it had a 97.5% accuracy for the mean flow in the y-direction with a divergence tolerance of 15° (Nitsche and Brunn, 2006). The measurement data were acquired using a USB-6361 DAQ device from the company National Instruments. For the measurements, the respective transducer was moved by an x–y-stage, while keeping the microphone or the hot-wire probe in the stationary position. For variations in the z-direction, the microphone was moved manually.

Microphone measurements were conducted in the negative z-range since reflectional symmetry was assumed. The sound measurements of the fluidic transducer had an offset of $z = 20$ mm from the acoustical axis. Placing the microphone into regions of high fluid velocities would lead to damage. The microphone data were corrected for directivity and frequency response of the measurement system. Flow measurements were conducted in the $z = 0$ mm plane only.

The process of switching *on* and *off* represents a full switching cycle, which is repeated 100 times at each measurement position. For the analysis of the acoustic field, four time intervals containing two switching events and two stable states were defined. The intervals were held constant for all cycles at all measurement positions. For switching events at a certain position, the maximum absolute pressure value $\hat{p}$ was picked from the previously defined intervals and averaged over all cycles. To determine the static noise level, the standard deviation of the acoustic pressure was calculated for the stable states, which is defined as

$$\overline{p'} = \sqrt{\frac{1}{N}\sum_i p_i^2}, \tag{2}$$

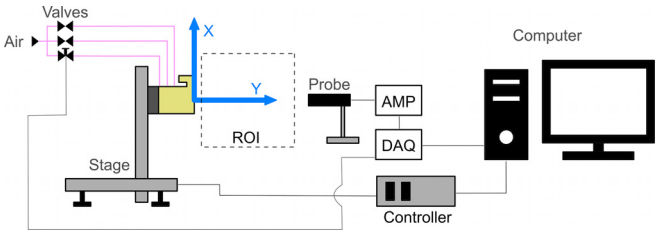

FIG. 3. (Color online) Experimental setup. Microphone, hot-wire probe, and Pitot tube were mounted at probe position.

where p_i are the sound pressure amplitudes and N is the number of samples. The data shows that 100 repetitions are sufficient for $\hat{p}$ and $\overline{p'}$ to converge.

IV. RESULTS AND DISCUSSION

The setup described above was used to measure the flow field and the acoustic field of a fluidic transducer. First, the acoustic field of a commercial piezoelectric transducer is investigated to provide a reference for the novel transducer design. Next, the flow field is described, whose characteristics are essential to the following discussion of the acoustic field of the fluidic transducer.

A. Piezoelectric transducer

An exemplary pulse of the piezo transducer, exhibiting a −40 dB pulse length of 300 μs, is shown in Fig. 4(a). The ultrasonic pulses have a center frequency of 82 kHz at a –6 dB bandwidth of 20 kHz, as shown in Fig. 4(b). The pulse length and bandwidth are in good accordance with previous measurements (Gräfe, 2009). The impulse response of the transducer exhibits a main lobe and side lobes in the frequency domain, which are not described by Gräfe (2009). This might be a result of the transducer's aging. Figure 4(c) shows the acoustic field of the transducer at the center plane and the sound pressure distribution along the acoustic axis. The distance of the focal point from the transducer surface is 220 mm, and the acoustic beam has a divergence of 5°, confirming the results obtained by Gräfe (2009) and Maack (2012). In the focal point the transducer generates a maximum sound pressure of 155 Pa. The high directivity is caused by the large transducer area compared to the generated wavelength of 4 mm.

B. Flow field of the fluidic transducer

The mean flow field of the fluidic switch in the *on* state is shown in Fig. 5(a). The maximum velocity of $u = 293$ m/s is reached closest to outlet 1, which is presumed to be the jet exit velocity. Although the inner channel leading to O1 is perpendicular to the exit plane, the measured jet shows an inclination of $\phi = 6°$. This behavior is believed to be a result of the monostable operation mode and a 4° inclination of the O1 channel with respect to the outlet plane. Nevertheless, during *off* state, a lower velocity at O1 is measured, with a maximum of $u = 1.5$ m/s, as shown in Fig. 5(b). As known from literature, this is a suction flow that develops if the flow is fully switched (Conway, 1971). The omnidirectional distribution around the outlet supports this assumption (Van Buren *et al.*, 2017).

C. Acoustic field of the fluidic transducer

Figure 6(a) shows a representative time signal of the acoustic pressure of two switching cycles, measured at $(x, y, z) = (0, 20, 40)$ mm. Additionally, four regions of interest, during both switching periods and in stable states, are highlighted. Both generated acoustic pulses can be

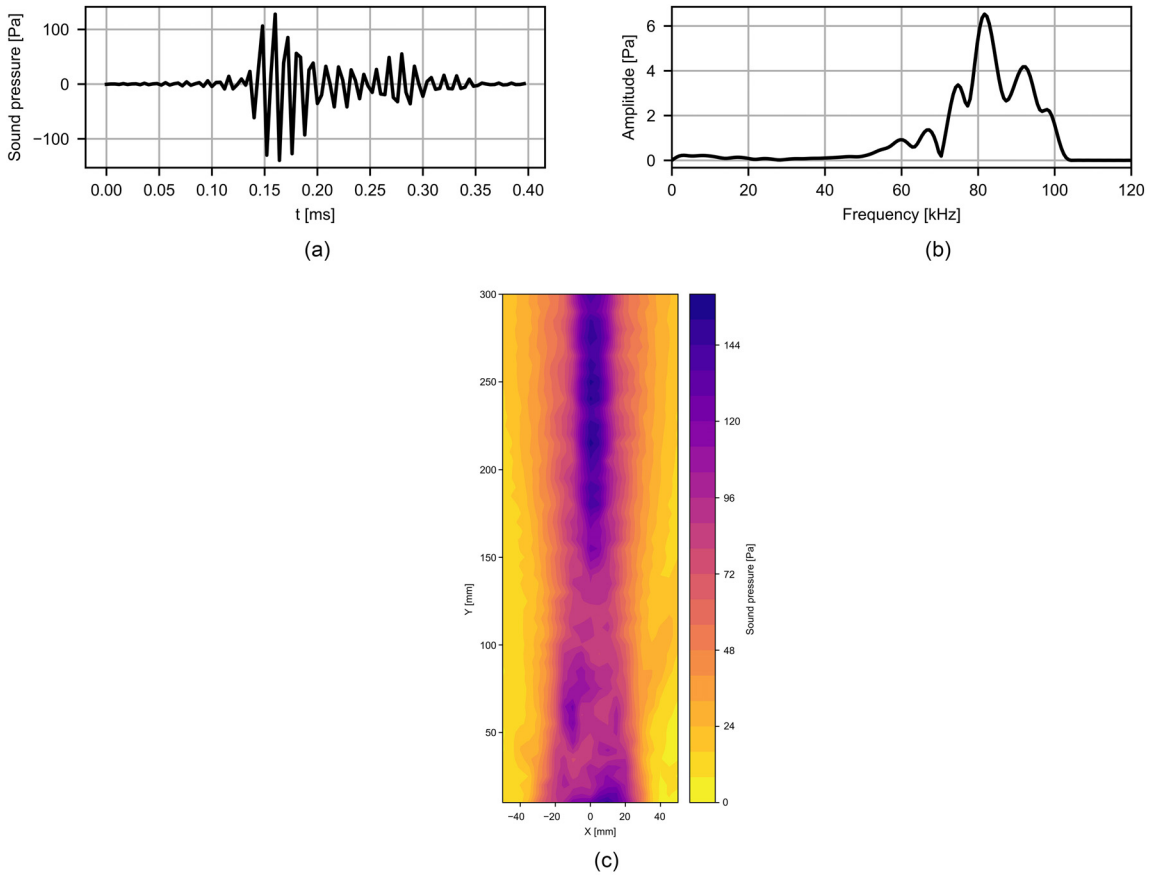

FIG. 4. (Color online) Acoustic field of the piezoelectric transducer. (a) Impulse response; (b) averaged time signal; (c) acoustic field.

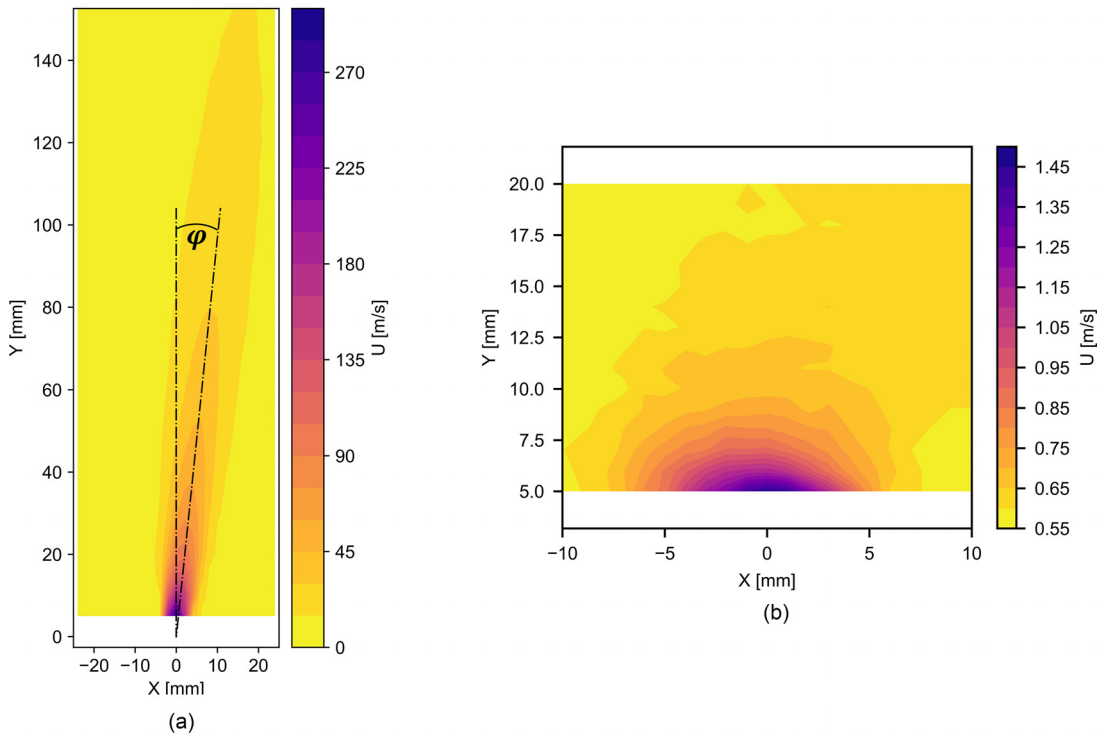

FIG. 5. (Color online) Flow field of the fluidic transducer. (a) *On* state; (b) *off* state.

https://doi.org/10.1121/10.0003937

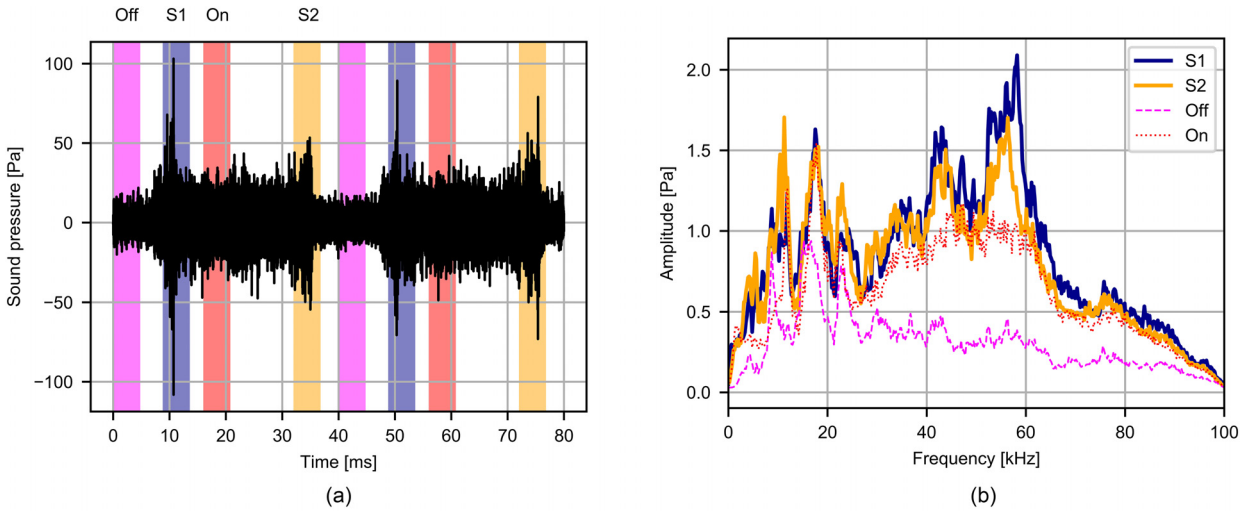

FIG. 6. (Color online) Representative signal generated by the fluidic transducer at $(x, y, z) = (0, 20, 40)$ mm. (a) Time signal of two switching cycles with intervals for analysis highlighted; (b) averaged impulse response in the highlighted intervals. S1, switching process 1; S2, switching process 2; On, *On* state; Off, *Off* state.

clearly distinguished from the sound emitted by the jet itself. Pulses vary in amplitude and location of the peak pressure, indicating variations in the internal dynamics of the fluidic switch. The frequency content of the highlighted time intervals averaged over 100 cycles is shown in Fig. 6(b). All intervals exhibit frequency peaks around 11.5, 17, and 22 kHz, which makes us assume that this is characteristic noise emitted steadily by the system. In the switching intervals (S1, S2), further frequency peaks are evident around 35, 42, and 56 kHz with bandwidths from 6 to 8 kHz. Although the pressure amplitude in the range of 30–65 kHz is slightly raised in the *on* state, the stationary flow exhibits no peaks in these intervals. This disparity shows that these ultrasonic components are only generated during fluidic switching. The pressure amplitude in the peak frequency range from 42 to 56 kHz exceeds the static noise in the *on* state by 30%–100%.

The acoustic fields of the four regions of interest averaged over 100 actuation cycles are shown in Fig. 7. These amplitudes are high-pass filtered with a threshold of 20 kHz to obtain solely the ultrasonic signal. For the switching intervals, the maximum absolute sound pressure $\hat{p}$ is displayed.

The ultrasonic field of the first pulse [Fig. 7(a)] exhibits a maximum of $\hat{p} = 162$ Pa at 5 mm axial distance from the outlet in the $z = 20$ mm plane. Higher values are expected on the jet axis. The field has a slightly elliptical directivity,

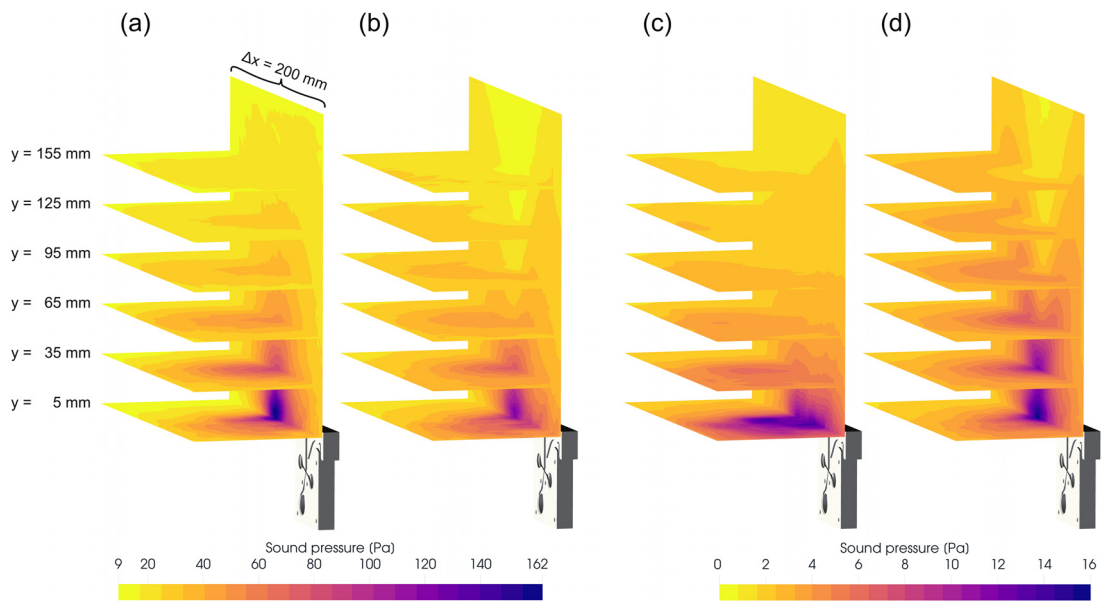

FIG. 7. (Color online) Averaged acoustic field of the fluidic transducer. (a) Switching process 1; (b) switching process 2; (c) *off* state; (d) *on* state. Note that the color scale for (a) and (b) is different from the color scale for (c) and (d).

which is consistent with analytical solutions for a finite piston in a rigid baffle with a *ka* value from 0.3 to 0.9, where a is substituted here with the hydraulic radius of the outlet.

The ultrasonic field of the second pulse shown in Fig. 7(b) exhibits a maximum of $\hat{p} = 121$ Pa at 10 mm axial distance from the outlet in the $z = 20$ mm plane. Contrary to the first pulse, the second one exhibits a hollow cone-shaped directivity. This divergence of the acoustic pressure maxima is related to the flow field shown in Fig. 5(a) and is consistent with the findings obtained by Choi *et al.* (2002), who describe the cone of silence developing when an air jet is used as an ultrasonic waveguide. A similar situation occurs when the second pulse is initiated. It is generated if the mass flow is suddenly switched *off* and enters the existing flow field established during the previous switching state. Shin *et al.* (2017) have shown that a free jet flow dissipates only at a timescale of 10^{-4} s, which is increasing in the flow direction. Thus, the flow field of the fluidic switch has no time to fully dissipate during the time of pulse generation. The speed of sound is not homogenous anymore and increases radially toward the jet axis. As a result, the emanating ultrasonic pulse diverges from the jet axis, as shown by Tam and Auriault (1998). In a further development, the defocusing effect of the jet may be reversed by altering its density through cooling or the use of a different working medium as shown by Choi *et al.* (2002).

Figures 7(c) and 7(d) show the level of static jet noise in the intervals of the *on* and *off* states. The maximum values are $\overline{p'_{on}} = 16$ Pa and $\overline{p'_{off}} = 14$ Pa. When switched *off*, the measured acoustic pressure has its maximum region close to the transducer surface with a slight shift in the direction of outlet 2. This sound is believed to be the jet noise emanating from the flow through outlet 2. The acoustic field in the *on* state has a hollow cone-shaped directivity as seen before in the case of the second pulse. Although the sound is generated by various mechanisms throughout the free jet, the same refraction mechanism applies.

V. CONCLUSIONS

This study examines the ultrasonic acoustic field of an ACU transducer based on a fluidic switch. For the first time, a pulsed free air jet has been used to generate an ultrasonic signal. A measurement setup has been designed to investigate both the acoustic field and the flow field throughout the switching cycle of the device. These results are compared to a commercial piezoelectric transducer for ACU.

The fluidic transducer generates peak frequencies around 35, 42, and 56 kHz; however, the generated pulse shape needs improvement since the non-uniformity of the peaks complicates precise time-of-flight measurements. When the mass flow is switched *on*, the transducer exhibits an elliptical directivity since its dimensions are of the same order of magnitude as the generated wavelengths. The ambient flow is a speed of less than 2 m/s and is directed to the transducer outlet so that it does not significantly influence the acoustic directivity. When switching *off* the transducer, the ultrasonic signal diverges from the acoustic axis forming a cone of silence. Here, the ultrasonic signal is ejected in a decaying free jet with a maximum centerline velocity close to the speed of sound. The maximum pressure amplitude generated by the fluidic transducer is slightly higher than the commercial piezoelectric transducer produces in its focal point.

The generated frequency range, the amplitude that can be achieved, and its robustness make the fluidic transducer presented here a promising tool for ACU inspection in civil engineering.

ACKNOWLEDGMENTS

The authors would like to thank Navid Nayeri from the Institute of Fluid Dynamics and Technical Acoustics at TU Berlin for support with the flow measurements, Mate Gaal (BAM 8.4) for support with the acoustic measurements, Stefan Facius (BAM 9.2) for manufacturing fluidic devices, and Eric Schönsee for helping with the data acquisition. This work was supported by the German Federal Ministry of Economics and Technology (BMWi) under the ZIM (Zentrales Innovationsprogramm Mittelstand) Grant No. ZF4044222WM7. Concept: B.B., C.S., S.M.; design of experiment: B.B.; transducer design: T.S.; data acquisition: B.B.; analysis: B.B.; validation: B.B., C.S., S.M.; original draft: B.B.; review and editing: C.S., S.M., T.S.; visualization: B.B.; supervision and administration: C.S., S.M.

Álvarez-Arenas, T. E. G., and Díez, L. (**2013**). "Novel impedance matching materials and strategies for air-coupled piezoelectric transducers," in *Proceedings of IEEE Sensors 2013*, November 3–6, Baltimore, MD, pp. 1–4.

Asadollahi, A., and Khazanovich, L. (**2018**). "Analytical reverse time migration: An innovation in imaging of infrastructures using ultrasonic shear waves," Ultrasonics **88**, 185–192.

Bente, K., Kotschate, D., Wendland, S., and Gaal, M. (**2018**). "The thermo-acoustic effect and its application in air-coupled testing of composite structures," in *Proceedings of the 10th International Symposium on NDT in Aerospace*, October 24–26, Dresden, Germany, pp. 1–8.

Berriman, J. R., Hutchins, D. A., Neild, A., Gan, T. H., and Purnell, P. (**2006**). "The application of time-frequency analysis to the air-coupled ultrasonic testing of concrete," IEEE Trans. Ultrason. Ferroelectr. Freq. Control **53**, 768–776.

Bobusch, B. C. (**2015**). "Fluidic devices for realizing the shockless explosion combustion process," Ph.D. thesis, Technische Universität Berlin, Berlin.

Bobusch, B. C., Woszidlo, R., Bergada, J. M., Nayeri, C. N., and Paschereit, C. O. (**2013**). "Experimental study of the internal flow structures inside a fluidic oscillator," Exp. Fluids **54**, 1–12.

Bovtun, V., Döring, J., Bartusch, J., Beck, U., Erhard, A., and Yakymenko, Y. (**2007**). "Ferroelectret non-contact ultrasonic transducers," Appl. Phys. A **88**, 737–743.

Bühling, B., Strangfeld, C., and Maack, S. (**2019**). "Entwicklung eines luftgekoppelten Ultraschall-Echo-Prüfverfahrens mittels fluidischer Anregung" ("Development of an air-coupled ultrasonic echo test method using fluidic actuation"), in *Proceedings of DACH-Jahrestag. 2019*, May 27–29, Friedrichshafen, Germany, pp. 1–8.

Chimenti, D. E. (**2014**). "Review of air-coupled ultrasonic materials characterization," Ultrasonics **54**, 1804–1816.

Choi, D. W., McIntyre, C., Hutchins, D. A., and Billson, D. R. (**2002**). "Gas jet as a waveguide for air-coupled ultrasound," Ultrasonics **40**, 145–151.

Conway, A. (**1971**). *A Guide to Fluidics* (Macdonald & Co., London).

Dai, X., Zhu, J., and Haberman, M. R. (**2013**). "A focused electric spark source for non-contact stress wave excitation in solids," J. Acoust. Soc. Am. **134**, EL513–EL519.
Daschewski, M., Boehm, R., Prager, J., Kreutzbruck, M., and Harrer, A. (**2013**). "Physics of thermo-acoustic sound generation," J. Appl. Phys. **114**, 114903.
Davies, S. J., Edwards, C., Taylor, G. S., and Palmer, S. B. (**1993**). "Laser-generated ultrasound: Its properties, mechanisms and multifarious applications," J. Phys. D: Appl. Phys. **26**, 329–348.
Gaal, M., Kotschate, D., and Bente, K. (**2019**). "Advances in air-coupled ultrasonic transducers for non-destructive testing," Proc. Mtg. Acoust. **38**, 030003–030007.
Gräfe, B. (**2009**). "Luftgekoppeltes Ultraschallecho-Verfahren für betonbauteile" ("Air-coupled ultrasonic echo method for concrete structures"), Ph.D. thesis, Technische Universität Berlin, Berlin.
Gräfe, B., and Krause, M. (**2006**). "Basic investigation with air-coupled ultrasonic echo for concrete elements," in *Proceedings of the NDE Conference on Civil Engineering*, August 14–18, St. Louis, MO, pp. 480–487.
Gregory, J. W., and Tomac, M. N. (**2013**). "A review of fluidic oscillator development and application for flow control," in *Proceedings of the 43rd Fluid Dynamics Conference*, June 24–27, San Diego, CA, pp. 1–17.
Hansen, S. T., Mossawir, B. J., Ergun, A. S., Degertekin, F. L., and Khuri-Yakub, B. T. (**1999**). "Air-coupled nondestructive evaluation using micromachined ultrasonic transducers," in *Proceedings of the IEEE Ultrasonics Symposium*, October 17–20, Caesars Tahoe, NV, pp. 1037–1040.
Hirsch, D., and Gharib, M. (**2018**). "Schlieren visualization and analysis of sweeping jet actuator dynamics," AIAA J. **56**, 2947–2960.
Hosten, B., Bacon, C., and Guilliorit, E. (**2002**). "Acoustic wave generation by microwaves and applications to nondestructive evaluation," Ultrasonics **40**, 419–426.
Hosten, B., and Bernard, P. A. (**1998**). "Ultrasonic wave generation by time-gated microwaves," J. Acoust. Soc. Am. **104**, 860–866.
Hutchins, D. A. (**1988**). "Ultrasonic generation by pulsed lasers," in *Physical Acoustics*, edited by W. P. Mason, and R. N. Thurston (Academic Press, San Diego, CA), pp. 21–123.
Hutchins, D., Burrascano, P., Davis, L., Laureti, S., and Ricci, M. (**2014**). "Coded waveforms for optimised air-coupled ultrasonic nondestructive evaluation," Ultrasonics **54**, 1745–1759.
Jacobs, L. J., and Whitcomb, R. W. (**1997**). "Laser generation and detection of ultrasound in concrete," J. Nondestr. Eval. **16**, 57–65.
Kim, K. Y., and Sachse, W. (**1983**). "X-ray generated ultrasound," Appl. Phys. Lett. **43**, 1099–1101.
Kirshner, J. M., and Katz, S. (**1975**). *Design Theory of Fluidic Components* (Academic Press, New York).
Koch, G. H., Brongers, M. P. H., Thompson, N. G., Virmani, Y. P., and Payer, J. H. (**2002**). "Corrosion cost and preventive strategies in the United States," Fhwa-RD-01-156, Fhwa, pp. 1–12.
Kotschate, D., Gaal, M., and Kersten, H. (**2018a**). "Acoustic emission by self-organising effects of micro-hollow cathode discharges," Appl. Phys. Lett. **112**, 154102–154104.
Kotschate, D., Gaal, M., and Kersten, H. (**2018b**). "Untersuchung der akustischen Eigenschaften von Plasmalautsprechern auf Basis einer dielektrischen gehemmten Oberflächenentladung (SDBD)" ("Investigation of the acoustic properties of plasma speakers based on surface dielectric barrier discharge (SDBD)", in *Proceedings of Daga 2018*, March 19–22, Munich, Germany, pp. 555–558.
Krautkrämer, J., and Krautkrämer, H. (**1990**). "Testing problems on non-metallic specimens," in *Ultrasonic Testing of Materials*, edited by J. Krautkrämer, and H. Krautkrämer (Springer, Berlin), pp. 514–527.
Kunert, U., and Link, H. (**2013**). "Verkehrsinfrastruktur: Substanzerhaltung erfordert deutlich höhere Investitionen" ("Transport infrastructure: Maintenance of assets requires significantly higher investments"), DIW-Wochenber. **80**(26), 32–38.
Kunkle, J., Vun, R., Eischeild, T., Langron, M., Bhardwaj, M., and Bhardwaj, N. (**2006**). "Phenomenal advancements in transducers and piezoelectric composites for non-contact ultrasound and other applications," in *Proceedings of the 9th ECNDT*, September 25–29, Berlin, Germany, pp. 1–7.
Laureti, S., Ricci, M., Mohamed, M. N. I. B., Senni, L., Davis, L. A. J., and Hutchins, D. A. (**2018**). "Detection of rebars in concrete using advanced ultrasonic pulse compression techniques," Ultrasonics **85**, 31–38.
Long, A. E., Basheer, P. A. M., Taylor, S. E., Rankin, B. G. I., and Kirkpatrick, J. (**2008**). "Sustainable bridge construction through innovative advances," Proc. Inst. Civ. Eng. Bridge Eng. **161**, 183–188.
Luukkala, M., Heikkila, P., and Surakka, J. (**1971**). "Plate wave resonance—A contactless test method," Ultrasonics **9**, 201–208.
Maack, S. (**2012**). "Untersuchungen zum schallfeld niederfrequenter ultraschallprüfkopfe für die anwendung im bauwesen" ("Investigations of the sound field of low-frequency ultrasonic probes for use in civil engineering"), Ph.D. thesis, Technische Universität Berlin, Berlin.
Maierhofer, C., Reinhardt, H.-W., and Dobmann, G. (**2010**). *Non-Destructive Evaluation of Reinforced Concrete Structures: Non-Destructive Testing Methods* (Elsevier, Amsterdam).
Mayer, K., Marklein, R., Langenberg, K. J., and Kreutter, T. (**1990**). "Three-dimensional imaging system based on Fourier transform synthetic aperture focusing technique," Ultrasonics **28**, 241–255.
McBride, S. L., and Hutchison, T. S. (**1976**). "Helium gas jet spectral calibration of acoustic emission transducers and systems," Can. J. Phys. **54**, 1824–1830.
Nitsche, W., and Brunn, A. (**2006**). *Strömungsmesstechnik (Flow Measurement Techniques)* (Springer, Berlin-Heidelberg).
Pierce, A. D. (**2007**). "Basic linear acoustics," in *Springer Handbook of Acoustics*, edited by T. D. Rossing (Springer, New York,), pp. 25–111.
Pierce, A. D. (**2019**). "Radiation from vibrating bodies," in *Acoustics: An Introduction to Its Physical Principles and Applications*, edited by A. D. Pierce (Springer International Publishing, Cham), pp. 177–239.
Popovics, S., Bilgutay, N. M., Caraoguz, M., and Akgul, T. (**2000**). "High-frequency ultrasound technique for testing concrete," ACI Mater. J. **97**, 58–65.
Purnell, P., Gan, T. H., Hutchins, D. A., and Berriman, J. (**2004**). "Noncontact ultrasonic diagnostics in concrete: A preliminary investigation," Cem. Concr. Res. **34**, 1185–1188.
Qiu, Y., Gigliotti, J. V., Wallace, M., Griggio, F., Demore, C. E., Cochran, S., and Trolier-McKinstry, S. (**2015**). "Piezoelectric micromachined ultrasound transducer (PMUT) arrays for integrated sensing, actuation and imaging," Sensors **15**, 8020–8041.
Rechten, A. W. (**1976**). *Fluidik: Grundlagen, Bauelemente, Schaltungen (Fluidics: Basics, Components, Circuits)* (Springer, Berlin-Heidelberg).
Robertson, E., Samant, P., Trevisi, L., Ji, X., and Xiang, L. (**2020**). "X-ray induced acoustic computed tomography," Photoacoustics **19**, 100177.
Schickert, M., and Krause, M. (**2010**). "Ultrasonic techniques for evaluation of reinforced concrete structures," in *Non-Destructive Evaluation of Reinforced Concrete Structures*, edited by C. Maierhofer, H.-W. Reinhardt, and G. Dobmann (Woodhead Publishing, Oxford), pp. 490–530.
Schickert, M., Krause, M., and Müller, W. (**2003**). "Ultrasonic imaging of concrete elements using reconstruction by synthetic aperture focusing technique," J. Mater. Civ. Eng. **15**, 235–246.
Shin, D.-H., Aspden, A. J., and Richardson, E. S. (**2017**). "Self-similar properties of decelerating turbulent jets," J. Fluid Mech. **833**, 1–12.
Shinoda, H., Nakajima, T., Ueno, K., and Koshida, N. (**1999**). "Thermally induced ultrasonic emission from porous silicon," Nature **400**, 853–855.
Spyropoulos, C. E. (**1964**). "A sonic oscillator," in *Proceedings of the Fluid Amplification Symposium*, May 26–28, Washington, DC, pp. 27–52.
Strangfeld, C., and Maack, S. (**2018**). "Method and device for analyzing a sample," U.S. patent DE102016120454-A1; WO2018077759-A1.
Tam, C. K. W., and Auriault, L. (**1998**). "Mean flow refraction effects on sound radiated from localized sources in a jet," J. Fluid Mech. **370**, 149–174.
Tang, S., Ramseyer, C., Samant, P., and Xiang, L. (**2018**). "X-ray-induced acoustic computed tomography of concrete infrastructure," Appl. Phys. Lett. **112**, 063504.
Tesař, V. (**2002**). "Microbubble generation by fluidics. Part I: Development of the oscillator," Colloq. Fluid Dyn., Prague, Czech Republic, 1-13.
Tesař, V. (**2007**). *Pressure-Driven Microfluidics* (Artech House, Boston, MA).

Van Buren, T., Smits, A. J., and Amitay, M. (**2017**). "Boundary layer suction through rectangular orifices: Effects of aspect ratio and orientation," Exp. Fluids **58**, 1–11.
Warren, R. W. (**1962a**). "Fluid oscillator," U.S. patent 3,016,066.
Warren, R. W. (**1962b**). "Some parameters affecting the design of bistable fluid amplifiers," in *Fluid Jet Control Devices: Papers Presented at the Winter Annual Meeting of the ASME*, edited by F. T. Brown (American Society of Mechanical Engineers, New York), pp. 75–82.
Woszidlo, R., and Wygnanski, I. (**2011**). "Parameters governing separation control with sweeping jet actuators," in *Proceedings of the 29th AIAA Applied Aerodynamics Conference*, August 18–21, Honolulu, Hawaii, pp. 1–19.